Natural Convection Around a Vertical Cylinder

Course Project

ME 4803 001 — Dr. M. Anderson

Paul Gessler
Marshall Schaeffer

Mechanical Engineering Department
Milwaukee School of Engineering

May 20, 2012

Abstract

In this course project, natural convection heat transfer was studied using a commercial computational fluid dynamics (CFD) software, ANSYS FLUENT. The buoyant flow around a vertically-oriented cylinder was allowed to develop from initially stagnant air. The simulation setup exploited the axisymmetric nature of the geometry. This assumption was valid because turbulent flow was not developed near the cylinder walls. Boundary conditions consisted of pressure inlets and outlets, an insulated wall, and constant-temperature walls at the cylinder surfaces.

Transient analyses were conducted to visualize the development of the buoyant plume. Mesh independence and boundary independence studies were conducted using steady analyses to reduce the required computation time. The eventual steady-state heat transfer rate was compared to empirical correlations and semi-analytical equations in several texts to validate the simulation. The total heat transfer rate in steady-state conditions predicted by ANSYS was 20.3 W, which agrees with both the semi-analytical and empirical correlations to within 20%.

1 Introduction

The heat transfer from a vertical, heated cylinder via natural convection into air was approximated using ANSYS FLUENT. The cylinder had a diameter of 0.08 m, a height of 0.10 m, and was at a constant temperature of 400 K. The ambient air was at a temperature of 300 K. Since laminar flow was anticipated (as explained in Section 3), which would mean no circumferential flow, an axisymmetric simulation was conducted. Solving the problem in an axisymmetric domain allowed for finer meshes and faster solutions. Figure 1 shows the domain and boundaries that were solved. The boundary on the left side

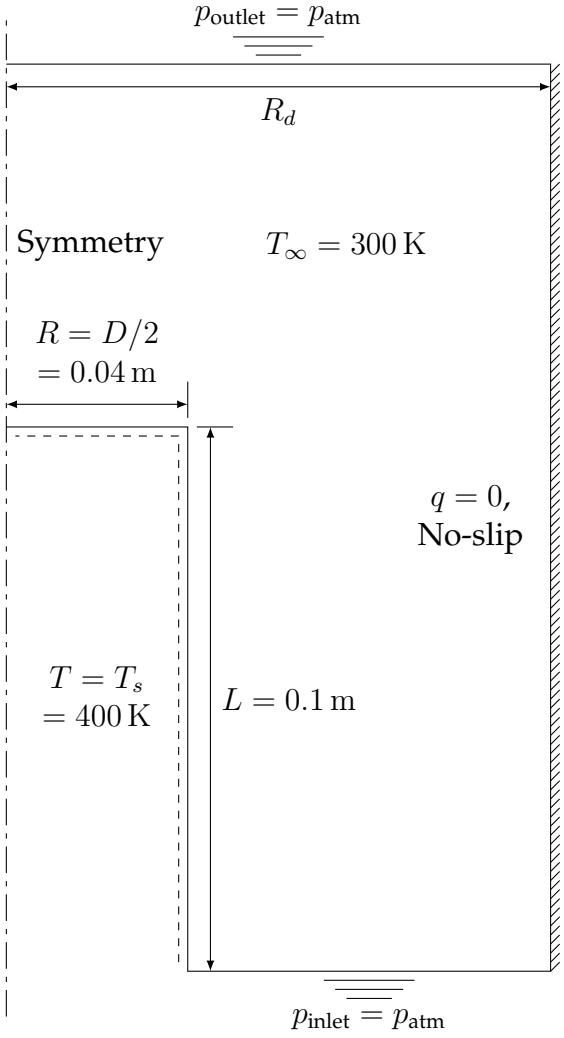

Figure 1: Simulation geometry and boundary conditions.

is the axis of rotation. An axis boundary condition was applied at this edge, which prevented flow from crossing the boundary but enforced no shear stress $\tau = 0$ in the fluid. The two boundaries with the dotted line are the cylinder top and side. These boundaries were no-slip walls assigned a constant temperature $T_s = 400\,\text{K}$. The boundary on the right was also a no-slip wall, but this wall was insulated ($q = 0$), allowing no thermal

energy exchange with the neighboring fluid. At the bottom and top of the domain were a pressure inlet and a pressure outlet, respectively. These boundaries allowed air to enter or leave as necessary to satisfy continuity.

A convergence study was performed to achieve mesh density independence and another study was performed to show independence of the distance from the axis to the wall pictured on the right in Fig. 1. The converged results were then compared to semi-analytical equations and empirical correlations to validate the numerical solution.

2 Solution Methodology

A number of tutorials and research works were consulted [1, 2, 3, 4, 5] to learn about fluid flow modeling in ANSYS FLUENT, specifically for buoyant flows such as those encountered when studying natural convection.

The ANSYS FLUENT Theory Guide [6] was consulted to learn about the solution techniques used within FLUENT. The following descriptions of the governing equations discretized by FLUENT for an axisymmetric domain are adapted from the Theory Guide [6].

Mass Conservation For the mass balance, FLUENT solves the general equation

$$\frac{\partial \rho}{\partial t} + \frac{\partial}{\partial x}\left(\rho v_x\right) + \frac{\partial}{\partial r}\left(\rho v_r\right) + \frac{\rho v_r}{r} = S_m, \tag{1}$$

where x is the axial coordinate, r is the radial coordinate, v_x is the axial velocity, v_r is the radial velocity, and the source S_m is used for multiphase flows only and represents the mass added to the continuous phase from the second phase. For the natural convection problem under consideration with a single phase, Eq. (1) becomes the homogeneous form

$$\frac{\partial \rho}{\partial t} + \frac{\partial}{\partial x}\left(\rho v_x\right) + \frac{\partial}{\partial r}\left(\rho v_r\right) + \frac{\rho v_r}{r} = 0. \tag{2}$$

Note that, for natural convection, incompressibility cannot be assumed since differences in density cause the buoyant forces driving the flow and allowing the convective heat transport.

Momentum Conservation In the conservation of momentum equations, FLUENT allows a swirl component of velocity v_z in the circumferential direction. For the laminar flow under consideration, we additionally assume no circumferential flow, causing all v_z terms in FLUENT's formulations to drop out, reducing to

$$\begin{aligned}\frac{\partial}{\partial t}\left(\rho v_x\right) + \frac{1}{r}\frac{\partial}{\partial x}\left(r\rho v_x^2\right) + \frac{1}{r}\frac{\partial}{\partial r}\left(r\rho v_r v_x\right) = &-\frac{\partial p}{\partial x} + \frac{1}{r}\frac{\partial}{\partial x}\left[r\mu\left(2\frac{\partial v_x}{\partial x} - \frac{2}{3}\left(\nabla\cdot\vec{v}\right)\right)\right] \\ &+\frac{1}{r}\frac{\partial}{\partial r}\left[r\mu\left(\frac{\partial v_x}{\partial r} + \frac{\partial v_r}{\partial x}\right)\right] + F_x\end{aligned} \tag{3}$$

and

$$\frac{\partial}{\partial t}\left(\rho v_r\right)+\frac{1}{r}\frac{\partial}{\partial x}\left(r\rho v_x v_r\right)+\frac{1}{r}\frac{\partial}{\partial r}\left(r\rho v_r^2\right)=-\frac{\partial p}{\partial r}+\frac{1}{r}\frac{\partial}{\partial x}\left[r\mu\left(\frac{\partial v_r}{\partial x}+\frac{\partial v_x}{\partial r}\right)\right] \\ +\frac{1}{r}\frac{\partial}{\partial r}\left[r\mu\left(2\frac{\partial v_r}{\partial r}-\frac{2}{3}\left(\nabla\cdot\vec{v}\right)\right)\right]-2\mu\frac{v_r}{r^2}+\frac{2}{3}\frac{\mu}{r}\left(\nabla\cdot\vec{v}\right)+F_r, \tag{4}$$

for the conservation of axial and radial momentum, respectively.

Energy Conservation When the energy equation is activated within FLUENT, heat transfer problems can be solved, such as the natural convection case examined in the present work. The energy equation formulation used within FLUENT is

$$\frac{\partial}{\partial t}\left(\rho E\right)+\nabla\cdot\left(\vec{v}\left(\rho E+p\right)\right)=\nabla\cdot\left(k_{\text{eff}}\nabla T-\sum_j h_j\vec{J}_j+\left(\bar{\bar{\tau}}_{\text{eff}}\cdot\vec{v}\right)\right)+S_h, \tag{5}$$

where $k_{\text{eff}}=k$ for the laminar flow studied herein, the summation of enthalpies h_j reduces to h since only one fluid is being studied, the effective stress tensor $\bar{\bar{\tau}}_{\text{eff}}=\bar{\bar{\tau}}$ since laminar flow is assumed, and $S_h=0$ since the flow is not chemically reacting with any other specie in this case. The stress tensor $\bar{\bar{\tau}}$ is given by

$$\bar{\bar{\tau}}=\mu\left[\left(\nabla\vec{v}+\nabla\vec{v}^{\text{T}}\right)-\frac{2}{3}\nabla\cdot\vec{v}I\right], \tag{6}$$

where μ is the viscosity and I is the unit tensor.

Body Forces The body forces which make natural convection possible are contained within the F_x and F_r terms of the momentum conservation equations in Eqs. (3) and (4), respectively. The contribution of the body force vector due to gravity is given by

$$\vec{F}_b=\rho\vec{g}, \tag{7}$$

where $\vec{g}$ is the gravitational acceleration vector with respect to the global x,r coordinate system.

Density Formulation Typically, a general flow analysis takes $\rho=$ constant to simplify the governing equations. In many cases, the effects of compressibility ($\rho\neq$ constant) are small and can be safely neglected. However, natural convection requires compressibility because without it, the body force would act equally on each differential element of fluid and could not cause bulk motion of the fluid. ANSYS has several methods of density calculation built-in. For this analysis, the ideal gas model was selected, since the fluid is air and the temperatures do not put the fluid into an extreme state. With the ideal gas model, the density ρ is computed using

$$\rho=\frac{p}{RT}, \tag{8}$$

where p is the pressure of the fluid, R is the gas constant specific to the fluid under consideration, and T is the fluid temperature in absolute units.

3 Mesh Size and Problem Feasibility

To determine a permissible range for the mesh spacing, the velocity boundary layer thickness along the side of the cylinder [7] was calculated using

$$\frac{\delta}{x} = 3.93 Pr^{-1/2} (.952 + Pr)^{1/4} Gr^{-1/4}, \tag{9}$$

where δ is the boundary layer thickness, x is the vertical distance along the cylinder face, Pr is the Prandtl number ($Pr = 0.7$ for air [8]), and Gr is the Grashof number. The Grashof number is defined by

$$Gr_x = \frac{g\beta \left(T_s - T_\infty\right) x^3}{\nu^2}, \tag{10}$$

where g is the acceleration of gravity, ν is the kinematic viscosity, and β is defined by Eq. (11) for an ideal gas.

$$\beta = \frac{1}{T} \tag{11}$$

Kays and Crawford [9] suggest using T_∞ as the temperature in Eq. (11), but it is also acceptable to use the film temperature (the average of the surface temperature and the ambient temperature). For this analysis, the film temperature was used. Equation (9) is for a flat plate but it can be applied to a vertical cylinder surface as long as Eq. (12) holds true.

$$\frac{D}{L} \geq \frac{35}{Gr^{1/4}} \tag{12}$$

The boundary layer thickness calculated was 0.016 m so the initial mesh spacing used was 0.001 m.

A calculation was also performed to check for turbulence. The transition to turbulent flow in natural convection is encountered at the critical Rayleigh number, which is approximately 10^9. Incropera and Dewitt [10] define the Rayleigh number by

$$Ra_x = Gr_x Pr. \tag{13}$$

The critical Grashof number for air, employing Eq. (13), is 1.43×10^9. The maximum Grashof number along the cylinder wall for the problem considered is 6.40×10^6, so the flow is laminar near the cylinder. This means that the problem can be solved using the laminar settings in ANSYS.

4 Results and Discussion

Complete steady-state results were obtained after conducting the mesh and boundary independence studies described in Sections 4.1 and 4.2. The final results for temperature, density, and velocity (magnitude contour and vector plot) are shown in Figs. 2 to 5. Note that the temperature (Fig. 2) and density (Fig. 3) contour plots are inversely related as expected based on the ideal gas model of Eq. (8).

Figure 2: Temperature contours at steady-state.

Figure 3: Density contours at steady-state.

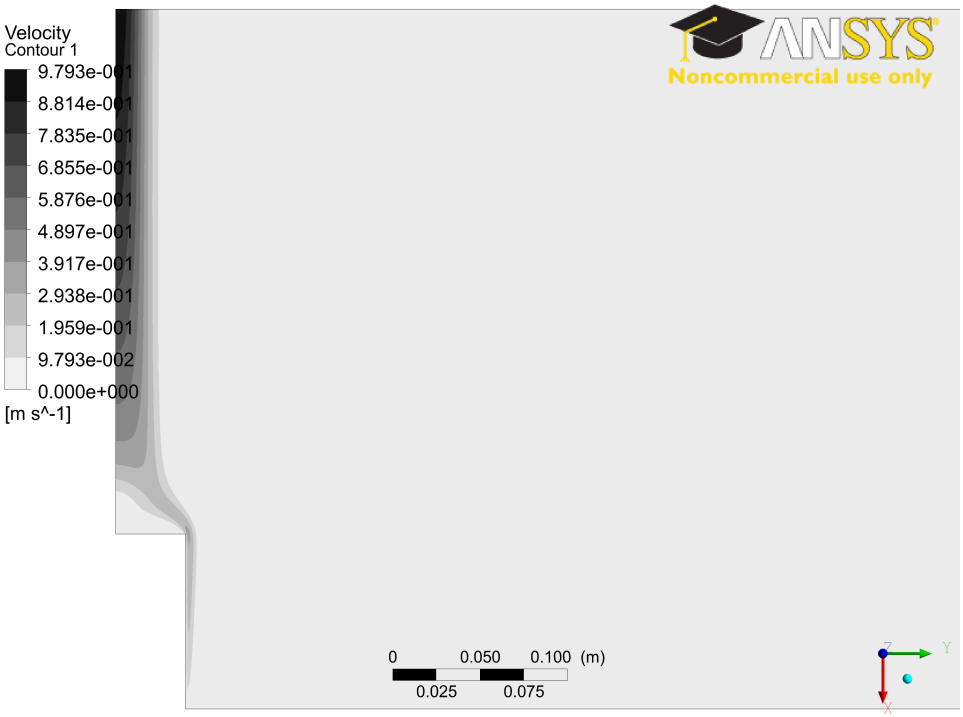

Figure 4: Velocity magnitude contours at steady-state.

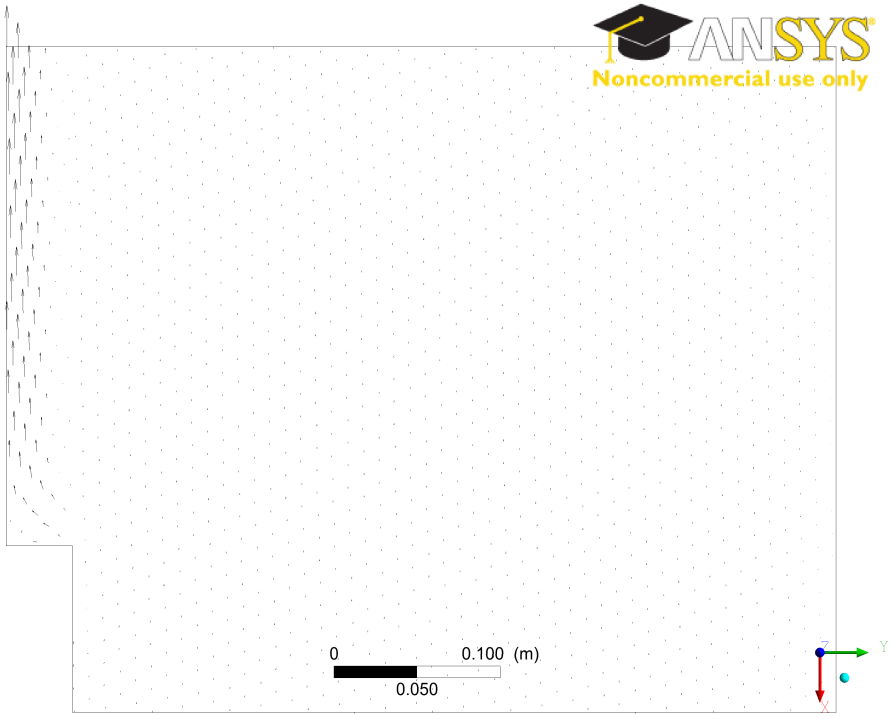

Figure 5: Velocity vectors at steady-state.

Streamlines of the steady-state solution near the top surface of the cylinder are shown in Fig. 6. Here, recirculation of the flow around the top of the cylinder is apparent. This shows an important interaction between the free convection off each surface which is not captured by the analytical or empirical methods. To investigate this difference, steady simulations were conducted which considered only one surface at a time. One surface was left at the elevated temperature $T_s = 400\,\mathrm{K}$ while the other was insulated. The results of these simulations are listed in Table 2.

Figure 6: Streamlines near the top surface of the cylinder. Note the closed shape resulting from recirculating flow.

4.1 Mesh Independence Study

To confirm the estimate of the required mesh size obtained using Eq. (9), a mesh independence study was conducted using 9 different cell edge lengths, ranging from 0.05 m at the coarsest to 0.00037 m at the finest. The finest mesh was selected to fall just under the cell count limit imposed by the educational version of ANSYS. The results of the mesh independence study are shown in Fig. 7. At cell edge lengths below 0.00075 m, the solution for the overall heat transfer rate differed by less that 0.2% in all cases.

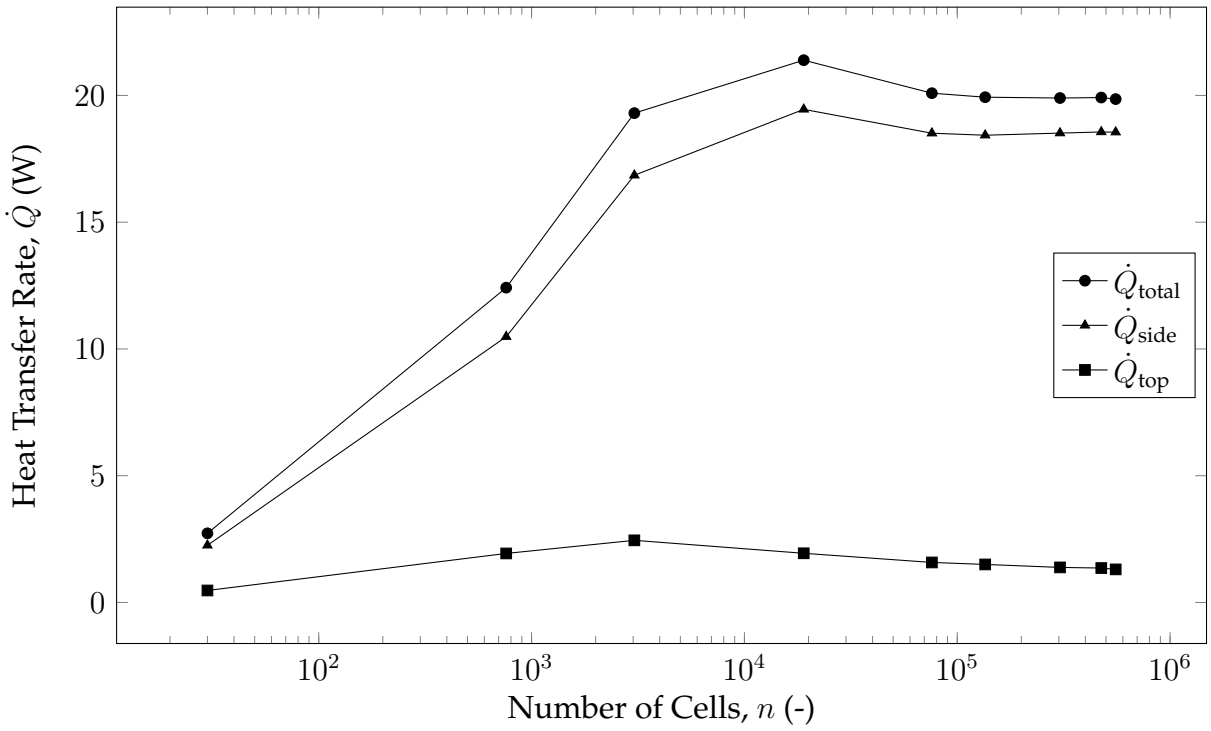

Figure 7: Mesh independence study results. Above $n \approx 10^5$, the solution is minimally affected by the mesh density. Note that the educational version of ANSYS FLUENT is limited to $n \leq 5.12 \times 10^5$.

4.2 Boundary Independence Study

To show that the presence of the insulated wall at the right side of the domain in Fig. 1 did not influence the heat transfer rate off the cylinder, the wall was moved further away from the axis in small steps. The results of the boundary independence study are shown in Fig. 8. Throughout the boundary independence study, all heat transfer rates agreed to within 1.5%.

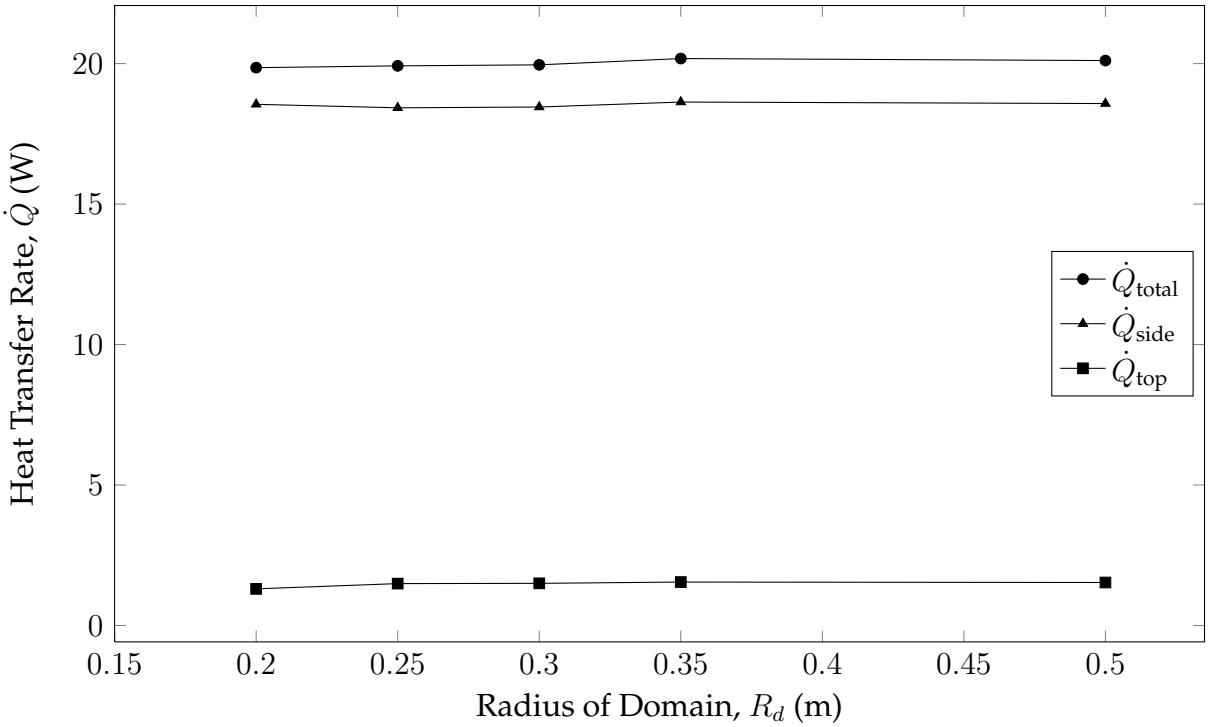

Figure 8: Boundary independence study results. The solution was influenced minimally by the insulated wall boundary in the range of domain sizes studied.

5 Validation and Discussion

The heat flow rates from the converged ANSYS models were compared to semi-analytical heat flow rate calculations for the purpose of validation. The average convection coefficient is $\bar{h}_c$, defined by

$$\bar{h}_c = \frac{\overline{Nu}_L k}{L}, \tag{14}$$

where $\overline{Nu}_L$ is the average Nusselt number (Eq. (15)), k is the thermal conductivity of the fluid taken at the film temperature, and L is the characteristic length of the geometry, in this case the length of the cylinder. As previously stated, the vertical cylinder wall is modeled as a vertical flat plate. The average Nusselt number $\overline{Nu}_L$ for a vertical plate is defined by Eqs. (15) and (16).

$$\overline{Nu}_L = \frac{4}{3}\left(\frac{Gr_L}{4}\right)^{1/4} f(Pr)\,, \tag{15}$$

where

$$f(Pr) = \frac{0.75Pr^{1/2}}{\left(0.609 + 1.221Pr^{1/2} + 1.238Pr\right)^{1/4}} = 0.499. \tag{16}$$

Kays and Crawford [9] note that the flat plate assumption is always conservative under the conditions when Eq. (15) is applicable. To correct the Nusselt number, Eq. (17) can be

applied if the Grashof number is low and the boundary layer thickness is significant in relation to the cylinder diameter. [9] This correction was applied to the Nusselt number for this problem because the boundary layer thickness was 0.0062 m, which is 7.5% of the cylinder diameter.

$$\overline{Nu}^* = \frac{2}{\ln\left(1 + \frac{2}{\overline{Nu}}\right)} \tag{17}$$

An empirical correlation [11] was also used to approximate the heat transfer rate from the sides of the cylinder. Equation Eq. (18) is also for a flat plate but can be applied to this specific cylinder since the condition of Eq. (12) is met. The value of $\overline{Nu}_L$ from this empirical correlation was also corrected using Eq. (17).

$$\overline{Nu}_L = 0.68 + \frac{0.670 Ra_L^{1/4}}{\left[1 + \left(\frac{0.492}{Pr}\right)^{9/16}\right]^{4/9}} \qquad Ra_L < 10^9 \tag{18}$$

The heat flow rate was calculated separately for the top of the cylinder. For a horizontal surface the average Nusselt number is

$$\overline{Nu}_L = 0.54 Ra^{1/4} \qquad 10^4 < Ra_L < 10^7, \tag{19}$$

and the Raleigh number is defined by

$$Ra_L = Gr_L Pr = \frac{g\beta\left(T_s - T_\infty\right) L^3}{\nu\alpha}. \tag{20}$$

For a horizontal surface a more accurate answer is achieved if L is defined by Eq. (21) instead of using a linear dimension of the surface. [10, 9] Since the top of the cylinder is circular, L can be represented by Eq. (22).

$$L = \frac{A_s}{P}, \tag{21}$$

or

$$L = \frac{\pi r^2}{2\pi r} = \frac{r}{2} = \frac{D}{4}. \tag{22}$$

The results from the converged ANSYS solutions are compared to the semi-analytical and empirical calculations in Table 1. Overall, the numerical solutions were within 20% of the calculated validation values. Note that for the heat flow rates through the cylinder side in Table 1 and Table 2, the Nusselt numbers were corrected using Eq. (17). The heat transfer rate off the side of the cylinder correlates to within 5% of the validation values, but the large difference in the heat transfer rate off the cylinder top suggests that the numerical model and the validation calculations describe different situations.

A possible explanation for the large discrepancy between the numerical and semi-analytical solutions for the heat flow rate off the cylinder top is the flow pattern. The semi-analytical equations employed are characteristic of flow that does not recirculate. In

Table 1: Overall heat transfer rate validation. Here, both surfaces of the cylinder were at an elevated temperature for the ANSYS analysis.

Heat Flow Rate (W)	Numerical (Steady)	Semi-Analytical	Percent Difference	Empirical Correlation	Percent Difference
Top	1.58	5.60*	112%	5.6	112%
Side	18.8	17.8	5%	19.1	2%
Total	20.3	23.4	14%	24.7	19%

* Semi-analytical equation was unavailable so the empirical correlation has been substituted.

the numerical solutions the air that comes off the cylinder side causes the flow at the top of the cylinder to swirl inward towards the center. This is likely to inhibit heat flow because the air at the top of the cylinder cannot escape. Figure 6 shows several streamlines showing trapped flow near the top surface of the cylinder. This trapped flow would act, in effect, like a thick boundary layer. In addition, the warm air coming off the side of the cylinder shields the top of the cylinder from the cool ambient air. Schaum's example problem solutions for natural convection off vertical cylinders did not include the horizontal cylinder top. [12] If the top surface is neglected for this problem and the side heat flux determined from the empirical correlations is compared to the total heat flux from the ANSYS simulation, there is only a 6% difference.

The effect that the warm air from the cylinder side has on the top is shown in Table 2 as the heat transfer off the top of the cylinder more than doubles when the sides of the cylinder are not heated in ANSYS. Even so, there is still a sizeable discrepancy with the empirical correlation. This may be because the empirical correlations are for a flat plate and not a cylinder. The cylinder walls may affect the flow to the top surface.

When the top of the cylinder is not heated in the ANSYS simulation, the numerical results match the semi-analytical and empirical calculations to within 4%.

Table 2: Individual surface heat transfer rate validation. Here, one surface is at an elevated temperature and the other is an insulated wall for the ANSYS analysis.

Heat Flow Rate (W)	Numerical (Steady)	Semi-Analytical	Percent Difference	Empirical Correlation	Percent Difference
Top	3.43	5.60[2]	48%	5.60*	48%
Side	18.6	17.84	4%	19.1	3%

* Semi-analytical equation was unavailable so the empirical correlation has been substituted.

6 Conclusions

The natural convection heat transfer rate off a vertical cylinder predicted by ANSYS FLUENT agreed with empirical and semi-analytical methods to within 20%. While this may

not seem like a phenomenally accurate result, the inexact art of convection heat transfer analysis (especially natural convection) means that the 'theoretical' validation conducted here may not actually recover the true solution. In addition, the equations used for validation are not generally applicable when convection off one surface affects another. For true validation of the solution for the heat transfer rate, physical experiments are required.

However, within the limited scope of the validation attempted here, the heat transfer rate predictions are very reasonable. The mesh independence and boundary independence studies confirmed that any errors in the simulations would be caused by the assumptions inherent in the simulation and not from numerical errors. The studies achieved this by showing that the simulations are not influenced by choices in problem setup, as long as reasonable values for cell edge length and wall distance are selected.

References

[1] ANSYS, INC., 2009. *ANSYS FLUENT 12.0: Tutorial Guide*. Canonsburg, PA. Release 12.0.

[2] ANSYS, INC., 2009. *Fluids Analysis Guide*. Canonsburg, PA. Release 12.1.

[3] CORNELL UNIVERSITY, 2011. *SimCafé: FLUENT Learning Modules*. Ithaca, NY. Release 12.1. URI: `https://confluence.cornell.edu/display/SIMULATION/FLUENT+Learning+Modules`.

[4] Fernández-Seara, J., Uhía, F. J., and Dopazo, J. A., 2011. "Experimental transient natural convection heat transfer from a vertical cylindrical tank". *Applied Thermal Engineering*, **31**(11), August, pp. 1915–1922.

[5] Popiel, C. O., Wojtkowiak, J., and Bober, K., 2007. "Laminar free convective heat transfer from isothermal vertical slender cylinder". *Experimental Thermal and Fluid Science*, **32**(2), November, pp. 607–613.

[6] ANSYS, INC., 2009. *Theory Guide*. Canonsburg, PA. Release 12.0.

[7] Rathmann, C., 2011. ME 318 Course Notes. Milwaukee School of Engineering.

[8] Munson, B., Young, D., Okiishi, T., and Huebsch, W., 2009. *Fundamentals of Fluid Mechanics*, 6th ed. John Wiley and Sons, Hoboken, NJ.

[9] Kays, W. M., and Crawford, M. E., 1980. *Convective Heat and Mass Transfer*, 2nd ed. McGraw Hill, New York.

[10] Incropera, F. P., DeWitt, D. P., Bergman, T. L., and Lavine, A. S., 2007. *Introduction to Heat Transfer*, 5th ed. John Wiley and Sons, Hoboken, NJ.

[11] Bejan, A., 1984. *Convection Heat Transfer*. John Wiley and Sons, Hoboken, NJ.

[12] Pitts, D. R., and Sissom, L. E., 1991. *Schaum's 1000 Solved Problems in Heat Transfer*. McGraw Hill, New York.